The molecular tweezer CLR01 inhibits aberrant superoxide dismutase 1 (SOD1) self-assembly *in vitro* and in the G93A-SOD1 mouse model of ALS

Ravinder Malik[1], Helen Meng[1], Piriya Wongkongkathep[2], Christian I. Corrales[1], Niki Sepanj[1], Ryan S. Atlasi[1], Frank-Gerrit Klärner[6], Thomas Schrader[6], Melissa J. Spencer[1,4], Joseph A. Loo[2,3,5], Martina Wiedau *[1,4], Gal Bitan*[1,4,5]

From the [1]Department of Neurology, David Geffen School of Medicine, [2]Department of Chemistry and Biochemistry, [3]Department of Biological Chemistry, [4]Brain Research Institute, [5]Molecular Biology Institute, University of California at Los Angeles, USA; [6]Faculty of Chemistry, University of Duisburg-Essen Essen, Germany.

Running Title: *CLR01 inhibits SOD1 aggregation in vitro and in vivo*

To whom the correspondence should be addressed: Gal Bitan, Department of Neurology, David Geffen School of Medicine, UCLA. E-mail: gbitan@mednet.ucla.edu, Tel: 310-206-2082 and Martina Wiedau, Department of Neurology, David Geffen School of Medicine, mwiedau@mednet.ucla.edu, Tel. 310-206-9933, Fax. 310-794-7491.

ABSTRACT

Mutations in superoxide dismutase 1 (SOD1) cause 15%–20% of familial amyotrophic lateral sclerosis (fALS) cases. The resulting amino-acid substitutions destabilize SOD1's protein structure, leading to its self-assembly into neurotoxic oligomers and aggregates, a process hypothesized to cause the characteristic motor-neuron degeneration in affected individuals. Currently, effective disease-modifying therapy is not available for ALS. Molecular tweezers prevent formation of toxic protein assemblies, yet their protective action has not been tested previously on SOD1 or in the context of ALS. Here, we tested the molecular tweezer CLR01—a broad-spectrum inhibitor of the self-assembly and toxicity of amyloid proteins—as a potential therapeutic agent for ALS. Using recombinant wild-type and mutant SOD1, we found that CLR01 inhibited the aggregation of all tested SOD1 forms *in vitro*. Next, we examined whether CLR01 could prevent the formation of misfolded SOD1 in the G93A-SOD1 mouse model of ALS and whether such inhibition would have a beneficial therapeutic effect. CLR01 treatment decreased misfolded SOD1 in the spinal cord significantly. However, these histological findings did not correlate with improvement of the disease phenotype. A small, dose-dependent decrease in disease duration was found in CLR01-treated, relative to vehicle-treated animals, yet motor function did not improve in any of the treatment groups. These results demonstrate that CLR01 can inhibit SOD1 misfolding and aggregation both *in vitro* and *in vivo*, but raise the question whether such inhibition is sufficient for achieving a therapeutic effect. Additional studies in other, less aggressive ALS models may be needed to determine the therapeutic potential of this approach.

Amyotrophic lateral sclerosis (ALS) is a rapidly debilitating neuromuscular disorder characterized by loss of motor neuron function in the spinal cord, brain stem, and motor cortex. The resulting progressive muscle weakness and atrophy leads to death typically occurring 3–5 years after onset. Approximately 90–95% of ALS cases are sporadic and the remaining cases

are familial (fALS), caused by mutations in multiple genes (1). More than 160 mutations in the SOD1 gene, encoding the enzyme superoxide dismutase 1 (SOD1), have been described to cause amino-acid substitutions that destabilize the protein leading to its aberrant self-assembly, which causes 15–20% of fALS cases (2).

SOD1 is a homodimer of a 153-amino acid polypeptide. The enzyme converts the superoxide ions produced by mitochondria into hydrogen peroxide. Some disease-associated SOD1 variants retain high activity (3) and the targeted deletion of SOD1 in transgenic mice does not induce ALS-like symptoms (4). Therefore, the mechanism by which mutant SOD1 causes ALS is believed to be not a loss of function, but rather a gain of toxic function upon misfolding and self-assembly into neurotoxic oligomers and aggregates (5,6). The latter are found in the brain and spinal cord of affected individual as intracellular inclusions.

To date, two drugs have been approved for treatment of ALS—riluzole (7) and edaravone (8). These drugs slow disease progression mildly but do not alter substantially the disease course. Thus, there is an urgent need for a disease-modifying therapy that would halt the progression and ultimately cure ALS. Inhibition and modulation of aberrant protein self-assembly are promising strategies for therapy development, which have been explored quite extensively for other proteinopathies, such as Alzheimer's disease (AD) and Parkinson's disease (PD) (9). In contrast, to date, few studies have examined small-molecule inhibitors of SOD1 self-assembly as a potential therapy for ALS. A study using pyrimidine-2,4,6-triones showed protection from SOD1-induced cytotoxicity in cultured cells (10). Using a different mechanism, restoration of cellular protein degradation by activation of the proteasome, pyrazolones have been found to protect PC-12 cells against the toxicity of G93A-SOD1 (11). In yet a third approach, in-silico screening

identified azauracil- and uracil-based inhibitors, which stabilized mutant SOD1 against aggregation in human plasma (12). The therapeutic efficacy of these compounds is yet to be tested in vivo. These few examples highlight the need for further exploration of strategies directed at misfolded SOD1 self-assembly as a potential target for ALS therapy.

SOD1 was the first gene linked to familial ALS (13). A transgenic mouse model of ALS, expressing human SOD1 containing a G93A substitution was first introduced in 1996 (14). Although this model is not ideal as it expresses a high copy number of the transgene and consequently displays highly aggressive disease progression, it has remained not only the most thoroughly characterized ALS animal model, but also has been regarded as the gold standard in preclinical therapeutic ALS research. This mouse model mimics motor neuron loss and progressive muscle weakness (15) similar to the clinical symptoms of human ALS. The mouse model has facilitated studying mechanistic aspects of the disease, yet the rapid course of disease may be too aggressive for many therapeutic approaches to have an effect.

Previously, we reported that molecular tweezers (MTs) are broad-spectrum inhibitors of abnormal protein self-assembly and toxicity (16-18). A lead MT, called CLR01 (Figure 3A), has been found to inhibit the formation of toxic oligomers and aggregates of multiple disease-associated proteins (19), including those involved in AD (20,21) and PD (22,23). CLR01 acts as a nanochaperone by a "process-specific" mechanism, i.e., it targets the process of abnormal protein self-assembly itself rather than a particular protein. CLR01 achieves this activity by labile binding to positively charged amino-acid residues, primarily Lys and to a lower extent Arg, temporarily reversing the charge from positive to negative and disrupting hydrophobic interactions in which the butylene moiety of the Lys side chain (or the propylene chain in the Arg side chain) participate. As hydrophobic and electrostatic interactions are

important, particularly in the early stages of the aberrant self-assembly process in which oligomers and aggregation nuclei form, MTs effectively interfere with the formation of these early assemblies.

CLR01 has been shown to have beneficial therapeutic effects in multiple animal models of various proteinopathies, including rodent models of AD (18,24), PD (25), TTR amyloidosis (26), and desmin-related cardiomyopathy (27). However, to date, MTs have not been explored in the context of ALS in general or for inhibition of the aggregation and toxicity of SOD1 in particular. Here, we evaluated the effect of CLR01 on SOD1 aggregation in vitro and in the G93A-SOD1 mouse model of ALS. Our data reveal that CLR01 inhibits the aggregation of wild-type and disease-associated variant SOD1 in vitro and reduces the accumulation of misfolded SOD1 in the mice. However, reduction of misfolded SOD1 did not result in significant therapeutic effects, possibly due to the fast disease progression in this model or due to other reasons discussed below.

Results
CLR01 inhibits the aggregation of wild-type (WT) and disease-associated SOD1

WT and variant SOD1 were expressed in yeast cells and purified using serial chromatography, as described previously (28). A eukaryotic yeast expression system is necessary for obtaining the correct posttranslational modifications of amino-terminal groups by acetylation (29). Each variant was de-metallated by incubation with excess EDTA and stored at -80 °C until use. The disease-associated variants included E21K, H46R, D76Y, and G93A. Aggregation kinetics were measured using the thioflavin-T (ThT) fluorescence assay and the morphology of the aggregates was visualized by electron microscopy (EM). To induce misfolding and monitor aggregation, 40 μM of each variant were incubated for 48 h at 37 °C in a 96-well plate with constant agitation in the presence of

50 mM tris(2-carboxyethyl)phosphine (TCEP) to reduce disulfide bonds and increasing concentration of CLR01. A Teflon ball was added to each well to facilitate the aggregation, as described previously (30).

In the absence of CLR01, all the variants showed a typical, time-dependent sigmoidal increase in ThT fluorescence consisting of an initial lag phase indicating misfolding and nucleation, followed by an exponential increase in fluorescence, and finally a plateau when most of the monomers have been exhausted (Figure 1A–E, red curve). In the presence of CLR01, dose-dependent inhibition of the aggregation was observed in all cases. The dose-dependence of the inhibition varied for the different isoforms but was complete or near complete at 5-fold excess CLR01 in all cases (Figure 1A–E, green curve).

Examination of the ThT curves showed that CLR01 affected all the stages of the aggregation process, including the lag phase (Supplementary Figure S1A), the slope of the exponential phase (Supplementary Figure S1B), and the final plateau (Supplementary Figure S1C), though the dose-dependence of the inhibition varied among the different variants. As shown in Figure 1 and Supplementary Figure 1, in some cases, e.g., WT SOD1, little inhibition was observed at 1:1 SOD1:CLR01 ratio, whereas in other cases, such as H46R-SOD1, substantial inhibition was found already with equimolar CLR01. The additional binding sites for CLR01 at K21 in E21K-SOD1 and R46 in H46R-SOD1 did not appear to play a major role in the activity of the compound. The exact mechanism underlying the differences among the SOD1 variants in not known and will require further investigation.

Morphological examination by EM showed that in the absence of CLR01, all the SOD1 variants formed primarily amorphous aggregates (Figure 1F–J). After long incubation (30–60 d), typical amyloid fibrils also were apparent (Figure 2). In the presence

of equimolar concentration of CLR01, smaller aggregates were observed (Figure 1K–O). This reduction of aggregate size was consistent in all cases, but did not correlate well with the ThT results. For example, in the cases of WT SOD1 or E21K-SOD1 the ThT change in the presene of equimolar CLR01 was similar to the control reactions in the absence of CLR01, yet the morphological examination showed substantially smaller aggregates, suggesting that these aggregates contained a high quotient of cross-β structures. At 5-fold molar excess of CLR01 only small amorphous structures were apparent, in agreement with a strong inhibition of the ThT-fluorescence increase (Figure 1P–T).

Previously, CLR01 was shown not only to inhibit the aggregation of amyloidogenic proteins, such as Aβ40, Aβ42 (19), and α-synuclein (22), but also to disaggregate pre-formed fibrils over several weeks when added at 10-fold excess. Here, we asked if it could also dissociate pre-formed fibrils or other aggregates of SOD1. To answer the question, we added 10-fold excess CLR01 and equimolar concentration of ThT to WT SOD1 or G93A-SOD1 that had been previously agitated at 37 ℃ for 48 h and then left at room temperature for 6 months. The mixtures were agitated at 37 ℃ for 26 d and ThT fluorescence was measured every 24 h. Aliquots from each reaction were taken on days 0, 10, and 26 for morphological examination by EM. The initial ThT fluorescence in the WT SOD1 reactions was ~20% higher than in the G93A-SOD1 reactions (Figure 2).

In both cases, the ThT fluorescence gradually decreased to about 50% of the original fluorescence value after ~20 days, at which point the value did not change anymore, suggesting that CLR01 dissociated some, but not all of the SOD1 aggregates. The morphological examination showed that at all time points, a mixture of fibrils and large and small amorphous aggregates was present, which did not show a clear trend of change

during the experiment, possibly due to the high morphological variability of the aggregates. This disagreement between the change observed by ThT but not by EM suggests that CLR01 can disrupt some, but not all of the cross-β structure of pre-formed SOD1 fibrils and/or amorphous aggregates under the experimental conditions we used.

Identification of the binding region of CLR01 on SOD1

SOD1 contains 11 Lys residues (12 in the E21K variant), each of which is a potential binding site for CLR01. Previous studies with amyloid β-protein (19), α-synuclein (23), huntingtin exon 1 (31), and tau (32) have shown that not all of these binding sites are equal and the molecular tweezer prefers certain Lys residues over others. Thus, we asked whether a preferred binding site for CLR01 also existed in SOD1. To answer the question, we used native mass spectrometry (MS) with electrospray ionization (ESI). These experiments showed that when SOD1 and CLR01 were mixed at a 1:1 ratio, the 1:1 complex was the predominant CLR01-bound stoichiometry; from the summed intensities of the peaks in the native ESI mass spectrum (Figure 3A), the relative ratios of the apo-, 1-ligand bound, and 2-ligand bound forms was 0.55:0.40:0.50. However, this does not preclude multiple binding sites for CLR01 on SOD1. By measuring the normalized signal intensities for each such complex, equilibrium dissociation constants were calculated using a Scatchard plot, as was done previously for α-synuclein (23). The first and second dissociation constants were measured to be 2.93 and 44.9 µM, respectively.

To elucidate the main binding site(s) of CLR01 on SOD1, we used tandem MS (MS/MS) or "top-down" MS of the protein-ligand complex. Using electron capture dissociation (ECD), covalent backbone bonds of the polypeptide could be cleaved while non-covalent forces holding the ligand bound to the

macromolecule were maintained. ECD-MS/MS of protein:ligand complexes yielded product ions from dissociation of the protein chain, some of which were still bound to the ligand. The sequence of these ligand-bound fragments was mapped onto the full-length protein sequence to determine the ligand binding region(s). The 12+-charged ion for the 1:1 SOD1-CLR01 complex was analyzed using this approach; protein fragments of the c- (retaining the N-terminus) and z- (retaining the C-terminus) product-ion series were detected. Some product ions from dissociation of the polypeptide backbone corresponded to unbound protein, whereas other product ions retained binding to CLR01 (Figure 3B, *dark lines*). The data was interpreted in a similar fashion as our previous work (19,23,33). CLR01 is bound to both the C-terminus retaining product ion z_{89} (cleavage between Phe_{64} and Asn_{65}) and the N-terminus retaining product ion c_{87} (cleavage between Val87 and Thr88, see Supplementary Table 1). These data allowed localizing the binding of CLR01 to the region SOD1(65–88), which contains two likely binding sites at Lys-70 and Lys-75. Arg-69 and Arg-79 also may be minor contributors to the binding in this region. The region is on the surface of the protein in the crystal structure (34) and thus readily available for CLR01 binding even before misfolding.

Examination of the impact of CLR01 on weight, muscle weakness, and respiration in the G93A-SOD1 transgenic mouse model of ALS

In view of the ability of CLR01 to inhibit the aggregation of SOD1 in vitro, we wanted to determine its impact on SOD1 aggregation in the G93A-SOD1 mouse model (14). Mice were treated with 0.5 or 5.0 mg/kg CLR01 administered by a daily subcutaneous (s.c.) injection. A control group was treated with vehicle (sterile saline). According to the standardized instructions of Prize4Life (http://www.prize4life.org), which provided the mice for the study, the treatment started at

50 days of age and continued until the mice met criteria for euthanasia due to advanced weakness. Each group comprised 12 female and 12 male mice.

Most previous studies in models of neurodegenerative diseases used s.c. administration via osmotic minipumps (24-26). This approach offers continuous drug administration but is limited to 5–6 weeks. In addition, though the aqueous solubility of CLR01 is high (>10 mM), at the limit of solubility, the highest dose possible using the model-1004 minipump used previously is 1.2 mg/kg per day. The terms of the Prize4Life-supported study mandated that extension of life must be the primary outcome measure. As the G93A-SOD1 mice tend to develop disease at 110–120 days of age and die at 130–140 days of age, using the same pumps for this study was impractical. Therefore, we decided to administer CLR01 by a s.c. daily injection, as was done in a recent study using a desmin-related cardiomyopathy mouse model (27). In using this method of administration, we took into account that the plasma half-life of CLR01, 2–3 h, and its first-pass blood–brain barrier penetration, 2–3% (35), may limit the exposure of the target, G93A-SOD1, to the compound. However, we reasoned that the much slower clearance of CLR01 from the CNS relative to clearance from the plasma (35) might allow gradual accumulation of the compound in the CNS and increase target engagement.

In addition to recording disease onset and disease duration before mice reached criteria for euthanasia, every week of the study we weighed the mice, tested their strength using the grip-strength and rotarod (starting on week 13) tests, and measured unchallenged and challenged pulmonary function, as described previously (36,37). Body weight is a sensitive indicator of adverse treatment effects and in this model, also reflect motor impairment that occurs during disease progression. All the animals consistently gained weight up to 13-

weeks (males) or 14-weeks (females) of age, after which the weight began to decline (Figure 4A, B). During the entire treatment period, there were no significant differences among the treatment groups in weight, morbidity, mortality or signs of distress, suggesting that the treatment did not cause overt adverse effects in the mice.

In the grip-strength test, female mice began to show weakness on week 15 and males on week 14, in agreement with the known more aggressive course of disease in male mice in this model (38,39). There were no differences in weakness progression among the females in the three treatment groups (Figure 4C). In the males, a trend toward faster progression in the high-dose group and slower progression in the low-dose group was observed, yet the differences were not statistically significant. The rotarod test was performed starting on week 13 and showed a similar trend to the grip-strength test. There was a slight delay in onset of weakness in the females in the low-dose group and a trend toward slightly better performance of the males in this group, but these differences were not statistically significant.

Patients with ALS invariably develop respiratory muscle weakness and most die from pulmonary complications (40). Therefore, we used plethysmography to test whether the treatment would affect the pulmonary function of the mice. In this test, mice are placed in a chamber that allows them to breathe naturally, unrestrained and untethered. The system measures the small changes in the air that is exchanged in and out of the entire chamber because of the animal's respiration (36). Mice were given a hypercapnic challenge to increase tidal volume and frequency. Measurements were performed every week between week 13 and week 18. Similar to the grip-strength and rotarod tests, the values of both unchallenged and challenged expiratory and inspiratory volume were similar in the all three treatment groups and did not show significant differences (Supplementary Data).

Effect of CLR01 on Disease onset, disease duration, and survival

A Kaplan-Meier analysis of timing of disease onset did not show statistically significant differences among the groups (Figure 5A). A small trend toward delayed onset was observed in both female and male mice in the low-dose treatment group, but it did not reach statistical significance. Disease onset, determined by the first detectable sign of leg weakness—scissoring of the legs when lifted by the tail—was earlier by 6 days on average in male mice than in female mice (Figure 5B, $F_{(1, 66)} = 6.794$, $p = 0.011$) but was not significantly different among the treatment groups. There was no statistically significant difference in overall lifespan among any of the groups (Figure 5C).

Effect of CLR01 on SOD1 accumulation and inflammation in mouse spinal cord

Following treatment and euthanasia, spinal cords were harvested. However, due to the aggressive course of the disease in this model, most of the mice still did not fulfil the criteria for euthanasia on the day before their death and were found dead the next day, when their tissues had begun undergoing necrosis and therefore could not be used for immunohistochemistry (IHC) analysis. Therefore, only euthanized mice (N = 7 (vehicle), 6 (low-dose group), 7 (high-dose group)) were included in the IHC analysis. The anterior horn in the lumbar region of the spinal cord of these mice was analyzed by IHC for the presence of motor neurons (anti-NeuN antibody), total SOD1 (Ab16831), G93A-SOD1 (C4F6), misfolded SOD1 (10C12), and microglia (anti-Iba1). Monoclonal antibody (mAb) C4F6 previously was reported to recognize misfolded SOD1 (41,42). However, our own characterization has shown that this mAb recognizes specifically G93A-SOD1 regardless of misfolding (43). In contrast, we

found that mAb 10C12 was highly sensitive for misfolded SOD1 (both wild-type and the G93A variant) (43) and therefore used it to analyze this form of the protein.

NeuN staining showed that in most of the sections no motor neurons were left. In a few sections we found 1–2 surviving motor neurons but their low frequency indicated that in the vast majority of the mice the motor neurons degenerated completely or almost completely by the time the mice reached the criteria for euthanasia, precluding quantitative analysis. IHC analysis of total SOD1 using polyclonal antibody Ab16831, which recognizes both mouse and human SOD1, showed little difference among the treatment groups (Figure 6A–D), in agreement with the expectation that normal SOD1 is not affected by CLR01 treatment. C4F6 staining showed a dose-dependent trend towards reduction in G93A-SOD1, which did not reach statistical significance (Figure 6E–H). This trend may reflect a decrease in misfolded G93A-SOD1 in the treated mice, likely due to increased clearance of the misfolded protein, as was reported previously for α-synuclein in zebrafish treated with CLR01 (22). C4F6 does not recognize metallated G93A SOD1 (43), which could suggest that the decreased signal treated mice might reflect stabilization of the native, metallated form of the protein. However, based on the known mechanism of action of CLR01 (17), this is an unlikely explanation of the data. A significant, ~3-fold reduction was found in 10C12-reactive misfolded SOD1 (Figure 6I–L). The integrated fluorescence density in the vehicle-treated mice, was 81.9, compared to 29.8 in the low-dose group and 37.0 in the high-dose group, demonstrating that CLR01 engaged the target and reduced misfolded G93A-SOD1 in the spinal cord of the mice, in agreement to the inhibition of aggregation observed in vitro (Figure 1E, J, O, T). Finally, staining with anti-Iba1 suggested a trend toward a decrease in microglia density (Figure 6M–O, quantified as

total fluorescence per μm^2) in the high-dose group, but due to high variability, this effect was not statistically significant (Figure 6P).

Discussion

To date, the two Federal Drug Administration (FDA)-approved drugs targeting ALS only extend the survival by only ~3 months. These drugs have considerable side effects. Thus, developing disease-modifying agents for ALS is an urgent need and testing such therapy in transgenic mice is a crucial step in the drug-development process. Here, we tested whether the molecular tweezer, CLR01, which has been shown to inhibit the formation of toxic oligomers and aggregates in other diseases, would be effective against aberrant SOD1 self-assembly and therefore offer potential therapy for ALS. For initial in vitro testing, in addition to WT SOD1, we examined the variants E21K, H46R, D76Y and G93A, in which the disease-associated amino-acid substitutions are located in different regions along the SOD1 amino acid sequence. As expected, based on the broad-spectrum mechanism of CLR01, in all cases, we found that the molecular tweezer inhibited the aggregation of SOD1 dose-dependently, with complete or near complete inhibition at 5-fold excess CLR01 (Figure 1A–E). Interestingly, the two cases in which the aggregation was not inhibited at a 1:1 SOD1:CLR01 concentration ratio were the wild-type and E21K isoforms. E21K may require a higher concentration of CLR01 for inhibition of aggregation due to the presence of the extra binding site at K21 relative to the other isoforms. However, the observation that wild-type SOD1 required more CLR01 for inhibition than the aggregation-prone variants H46R, D76Y, and G93A is difficult to explain and will require further study. Morphological examination showed that inhibition of the ThT fluorescence increase correlated with inhibition of aggregation (Figure 1). As SOD1 contains 11 Lys residues, the Lys:CLR01 concentration ratio at the highest CLR01 concentration

corresponds to 2.2:1 (2.4:1 for E21K-SOD1), respectively, suggesting that when approximately half of the Lys residues are bound by CLR01, complete inhibition is achieved. It is important to remember, however, that the binding of CLR01 is highly labile, which means that at this concentration ratio, most of the Lys residues likely are bound part of the time.

To gain further insight into which Lys residues are most likely to be engaged by CLR01, we used top-down MS and determined that CLR01's main binding site was in the region comprising residues 65–88, which contains two Lys and two Arg residues. These experiments suggest that CLR01 binds preferentially to the Lys residues in positions 70 and 75. Previously, several regions in SOD1 have been reported to be important for the aggregation process, including residues 14–21, 30–38, 101–107, and 147–153 (44); 10–23, 92–122, and 137–153 (45). In addition, residues 28–38 have been suggested to be involved in mediating SOD1 toxicity, presumably in an amyloidogenic oligomer structure. The main binding sites of CLR01, K70 and/or K75 are not involved in any of these segments, which may explain why a five-fold excess of CLR01 is needed for complete or near-complete inhibition of SOD1 aggregation (Figure 1). Of the segments listed above, SOD1(30–38) contains two Lys residues, at position 30 and 36. These residues obviously are also in the segment implicated in toxicity—SOD1(28–38). In addition, K23 is at the C-terminus of SOD1(10–23), and K122 is at the C-terminus of SOD1(92–122). The other amyloidogenic segments do not contains Lys residues and therefore are not affected directly by CLR01. It is thus reasonable to hypothesize that the inhibitory activity of CLR01 is mediated by binding to K30 and/or K36, but binding to these residues likely occurs secondary to the binding of CLR01 to K70/K75, diminishing the effectivity of the molecular tweezer against SOD1.

In view of the ability of CLR01 to inhibit SOD1 aggregation in vitro, we hypothesized that it could be used therapeutically for fALS cases caused by mutant SOD1 and took the first step toward testing this hypothesis by treating the G93A-SOD1 mouse model with CLR01. This model is the most widely used and characterized mouse model for ALS, displaying typical symptoms of ALS, including progressive muscle weakness, weight loss, and difficulty with mobility, and has a 50% survival rate at 128.9±9.1 days (14).

As expected, misfolded SOD1 detected by mAb 10C12, which we have found recently to be highly sensitive to early SOD1 misfolding, was reduced by ~3-fold ($p < 0.01$) in the spinal cord of the CLR01-treated mice compared to vehicle-treated mice (Figure 6I–L). Interestingly, the reduction was similar in both treatment groups, suggesting that 0.5 mg/kg daily injection of CLR01 achieved maximal target engagement. The reduction in misfolded SOD1 correlated with a decrease in G93A-SOD1 measured using mAb C4F6 (Figure 6 E–H), but not total SOD1 (Figures 5A–D).

Despite the significant decrease in misfolded SOD1, the treatment did not affect significantly the loss of motor neurons and the ensuing rapidly progressive weakness leading to death of the mice (Figures 4A, C). Interestingly, one male mouse in the 0.5-mg/kg group deviated significantly from the rest, lived until 165 days of age, and started showing a decline in rotarod performance only on week 22 (Figure 4F). However, it is not known whether the treatment contributed to the extension of life and slower decline in this mouse. Most mice showed initial signs of weakness starting on day 110–120 (Figure 4C-F) and subsequently their disease progressed for ~1–4 weeks until they either fulfilled the criteria for euthanasia or died. There was a small delay of the disease onset in the mice receiving 0.5 mg/kg CLR01. In contrast, male mice receiving 5.0 mg/kg CLR01 appeared to

have an earlier onset and a more severe progression (Figure 5A–C).

Male mice consistently showed earlier disease onset than female mice, as reported previously (14). This was readily observed in the grip-strength (Figures 2C, D) and rotarod (Figures 2E, F) tests, in which the males showed earlier signs of motor difficulty than the females. Consequently, the male survival was shorter than that of the females (Figure 5A). CLR01 caused a more rapid decline in the performance of the male mice in the grip-strength and rotarod tests, whereas 0.5 mg/kg caused a small delay (Figures 2D, F). These trends did not reach statistical significance and were not observed in female mice. Nonetheless, because they were observed consistently in a number of tests, they do suggest that CLR01 treatment may be beneficial at lower doses and serve as a cautionary note for the use of higher doses. It is not clear at this point if these effects are specific to the G93A-SOD1 mice or are more general.

Toxicity studies in wild-type mice showed that CLR01 had a high safety margin. A single dose of intraperitoneal (i.p.) 100 mg/kg CLR01 caused temporary distress due to liver injury (35), as would be expected for such a high dose, but the symptoms resolved completely within 2 h without any mortality (N = 8). Daily administration of 10 mg/kg CLR01 i.p. for 30 days had a single significant effect of ~40% reduction of plasma cholesterol, but no other effects on mortality, morbidity, general behavior, histology, or serology (35). In view of these results, it is unlikely that the slight adverse effects observed upon daily administration of 5.0 mg/kg s.c. reflected general toxicity.

The discrepancy between the observed clearance of misfolded SOD1 (Figures 4I–L) and lack of significant effect on the motor tests or the disease course was surprising. One possible explanation of the results is that

misfolded SOD1 is not the cause of the disease in fALS or at least in this mouse model. Though we cannot rule out this possibility, it would contradict a large body of literature without providing an explanation for the cause of the disease (46). Alternative explanations are: 1) the high-copy overexpression of the SOD transgene in the G93A mouse causing a rapid disease progression, which cannot be counteracted by aggregation inhibitors, such as CLR01; 2) insufficient Cu^{2+} levels in the brain due to the high copy overexpression of the transgene, which is unaffected by CLR01; 3) the sub-optimal route of administration, which might have limited target exposure; and 4) formation of toxic SOD1 structures that are unaffected by CLR01. If build-up of CLR01 in the CNS was slower with daily injection than using continuous administration via pumps, as was done previously, the amount of compound available for preventing formation of toxic SOD1 assemblies might have not been sufficient in the high-copy-number, aggressive G93A-SOD1 model. The non-discriminatory nature of CLR01's mechanism of action, which is based on binding to exposed Lys and Arg residues regardless of assembly state, and the presence of 11 Lys and 4 Arg residues in SOD1, make the existence of putative, specific forms that are unaffected by CLR01 unlikely. The successful improvement of the disease phenotype in this mouse model following treatment with $Cu^{II}(atsm)$ (47) supports the possibility that Cu^{2+} depletion, rather than misfolded G93A-SOD1, was a major contributor to the pathological process in the mice. Finally, it is not possible to formally exclude the possibility that CLR01 treatment converted SOD1 into toxic structures that are not recognized by mAb 10C12. If this is the case, it would contradict all the studies reported so far using CLR01 in cell culture or *in vivo*, which showed beneficial effects of the compound. We hypothesize that examination of CLR01 or other molecular-tweezer derivatives with improved pharmacokinetic

9

characteristics in a model with slower progression may lead to a better outcome on disease onset and mouse survival.

Experimental Procedures

Materials. Thioflavin T (ThT), tris (2-carboxyethyl)phosphine (TCEP), ethylenediaminetetraacetic acid (EDTA), sodium acetate, sodium chloride, and other high purity reagents and buffers were obtained from Sigma-Aldrich or Thermo Scientific. The Na^+ salt of CLR01 was prepared and purified as described previously (48). The compound was dissolved in a sterile-saline solution for administration to animals.

Yeast Expression System. EG118 yeast cells, a deletion mutant for yeast *sod*1 (*sod*1Δ) (49), were transformed with YEp351, a yeast multicopy shuttle vector containing a LEU2 selectable marker and WT or mutant human SOD1 gene (50). Plasmids containing sequences for WT and SOD variants G93A, E21K, H46R and D76Y were a kind gift from Dr. Joan Valentine, UCLA.

Mouse Model. Transgenic B6SJL-Tg mice hemizygous for G93A-SOD1, used in this study were obtained through Prize4Life from Jackson Laboratory. Animal care was provided in accordance with the United States Public Health Service Guide for the Care and Use of Laboratory Animals. All procedures were approved by the Institutional Animal Care and Use Committee of the University of California, Los Angeles.

Antibodies. Antibodies and dilutions: Rabbit pAb ab16831 (1:1,000) was obtained from Abcam. Mouse mAb C4F6 (1:250) mouse was from MédiMabs, Montréal, Québec, Canada. Mouse mAb 10C12 (1:500) was a generous gift from Dr. Neil Cashman, University of British Columbia, Canada. Guinea-pig pAb anti-Iba1 (1:250) was from Synaptic Systems, Göttingen, Germany. Biotinylated anti-rabbit IgG (1:500, Vector Labs), Alexa Fluor 488-labeled anti-mouse IgG

(1:500) and Alexa Fluor 594-conjugated anti-guinea-pig IgG (1:2,500, Fisher Scientific) were used as secondary antibodies.

Protein Purification and Demetallation. EG118 *Saccharomyces cerevisiae* were transformed with each plasmid. Yeast cells were grown at 30 °C with 220-rpm shaking in yeast extract-peptone or synthetic dropout without Leu, containing 2% glucose. The culture was grown for 5–7 days until reaching $OD_{600} = 0.6$–0.9. Then, cells were resuspended in a double volume of lysis buffer containing 250 mM Tris-HCl, 150 mM NaCl, and 0.1 mM EDTA, pH 8.0. Cells were lysed by adding 0.5-mm glass beads and vortexing in a blender at high speed. Proteins were purified using sequential hydrophobic-interaction, ion-exchange, and size-exclusion chromatographies, as described previously (51). The de-metallated (apo) form of each variant was obtained by dialyzing first against 50 mM EDTA, 100 mM sodium acetate, pH 3.8, then against 100 mM NaCl, 100 mM sodium acetate, pH 3.8, and finally against 10 mM potassium phosphate, pH 7.0. The concentration of the proteins was determined by measuring absorbance at 280 nm using $\varepsilon = 10,800\ M^{-1}\ cm^{-1}$ at $\lambda = 280$ nm.

Thioflavin T (ThT) Assay. De-metallated variants of SOD1 were incubated at 40 µM in the absence or presence of 40 or 200 µM CLR01in a buffer containing 10 mM potassium phosphate, 40 µM ThT, and 50 mM TCEP, pH 7.4. The aggregation reactions were carried out in 96-well plates, each containing a final volume of 100 µL and a teflon ball to assist with agitation. Triplicate samples were incubated at 37 °C with agitation at 300 rpm in a plate reader (Synergy HTX, BioTek Instruments) in three independent experiments. ThT fluorescence was measured every 10 min using $\lambda_{ex} = 420$ nm $\lambda_{em} = 485$ nm (52). For clarity, data points are presented only every 30 minutes in Figure 1.

Transmission Electron Microscopy. Ten-µl aliquots were taken at the end of each aggregation reaction and applied onto freshly glow-discharged, carbon-coated, 400-mesh copper grids, rinsed with deionized water, and stained with 1% uranyl acetate, as described previously (28). Images were obtained using a JEOL JEM1200-EX transmission electron microscope at 80 kV.

Remodeling of SOD1 aggregates by CLR01. Forty-µM WT SOD1 or G93A-SOD1 were aged for 6 months. The pre-formed aggregates were mixed with 10-fold excess CLR01 in a 96-well plate and covered with a sealing film to avoid evaporation. Triplicate samples were incubated at 37 °C without agitation. ThT fluorescence was measured every 24 h using $\lambda_{ex} = 420$ nm $\lambda_{em} = 485$ nm (52). The samples were shaken for 20 s in the plate reader (Synergy HTX, BioTek Instruments) each time before taking the reading. Ten-µL aliquots taken on day 0, 10 and 26 for morphological analysis by EM.

Native mass spectrometry. Native electrospray ionization-mass spectrometry was performed using a Bruker Solarix 15-Tesla FT-ICR mass spectrometer (Billerica, MA), equipped with an Infinity ICR cell. Protein solutions were prepared at a concentration of 5–10 µM in 20 mM ammonium acetate, pH 6.8. Samples were loaded into a borosilicate glass capillary coated with Au/Pd (Proxeon) for nanoelectrospray. The analyte solution flow rate was 50–100 nL/min. The ESI voltage was set to 1.1 kV. Drying gas was applied at 0.5 L/min at 160 ºC in the ESI source region to aid desolvation. Transfer ion optics were tuned to the following settings: capillary 200 V, deflector plate at 180 V, funnel 120 V, skimmer 40 V. For top-down MS experiments, the ECD parameters were the following: 10 ms electron pulse, a 1 V bias, and 15 V applied to the lens. Product ions were manually identified using the Bruker DataAnalysis software and assigned by a home-built Matlab program using a ≤10 ppm mass accuracy tolerance.

Mouse treatment. G93A-SOD1 transgenic mice were kept in standard mouse housing with 12-h light/dark cycles and ad libitum chow and water. Daily s.c. injections of CLR01 started at 50 days of age. Treatment ended when the mice met either one of the criteria for euthanasia: either loss of ≥10% of body weight or inability of the mouse to right itself within 30 s when placed on either of its sides.

Experimental Groups. The cohort comprised 72 mice – 36 males and 36 females, which were randomized into three treatment groups receiving 0, 0.5, or 5.0 mg/kg CLR01 in 0.9% (w/v) sterile saline by daily s.c. injection. Each group included 12 females and 12 males. The mice were weighed and tested for strength using the grip-strength and rotarod tests weekly. In addition, the respiratory volumes of the mice under normal and challenging conditions (elevated CO_2) were measured weekly.

Grip-strength test. The test started on week 7. Each mouse was placed on a wire lid of a conventional housing cage and the lid was turned upside down. The latency from the beginning of the test until the mouse stood with at least two limbs on the lid was timed. The animals had three attempts to stand for a maximum of 60 s each for 5 trials and the longest latency was recorded.

Rotarod Test. Mice started training on the rotarod apparatus daily one week before data recording began on week 13. Animals were placed onto the cylinder at a constant speed of 15 rpm for 5 min. The longest latency to fall in 3 trials was recorded for up to 300 s per trial.

Pulmonary function. The inspiratory and expiratory flow were measured in conscious, unrestrained mice using a whole-body plethysmograph (Buxco, Data Sciences International). The system measures the small changes in the air that is exchanged in and out of the entire chamber due to the animal's respiration. The chamber was calibrated before every experiment, selecting the most

11

appropriate response observed in FinePoint Software (Buxco, Data Sciences International) to the injection of 1 ml air into the chamber. After calibration, mice were placed into the chamber and acclimated for 55 min. CO_2 concentration was maintained during the acclimation and room-air breathing periods by using a bias-flow regulator. After acclimation, baseline respiratory function was measured for 5 min. After baseline correction, bias flow was turned down for the first CO_2 exposure. The bias flow was turned back on for 10 min and again turned off for the second CO_2 exposure. Both exposures used 4 mL CO_2 for 5 min. All data were collected and analyzed using FinePoint, which uses algorithms that include variables affecting respiratory function, such as humidity and temperature, to calculate the measured box flow and the physiological values of the respiratory parameters from the animal.

Immunohistochemistry. Euthanized animals were perfused with 4% paraformaldehyde. Spinal cords were removed and post-fixed for 2 h in 4% paraformaldehyde. Thereafter the tissue was dehydrated, paraffinized, and sectioned. To prepare the lumbar spinal cord sections for immunohistochemistry analysis, all slides were incubated at 50–60 °C for 60 min. Slides then were deparaffinized by soaking the sections in xylene four times and rehydrated sequentially in 100%, 95%, and 70% ethanol. Antigens were retrieved by placing sections in 10 mM sodium citrate buffer, pH 6.0, and heating in a pressure cooker for 10 min and allowed to cool back down to 20 ºC. Sections then were washed in 0.05% (v/v) Tween-20 in PBS, blocked in 5% (v/v) normal goat serum (NGS) in PBS, and incubated with each primary antibody in 2.5% (v/v) NGS in PBS at the dilutions mentioned above. Sections stained with Ab16831 were subsequently washed and incubated with a biotinylated anti-rabbit secondary antibody in wash buffer. Slides were then incubated with an avidin:biotinylated enzyme complex (ABC

Elite Vectastain kit, Vector Labs) using a peroxidase detection system for 80 min at 37 ºC as described previously (24). Antigen was visualized by incubation for 2 min with metal-enhanced 3,3'-diaminobenzidine tetrahydrochloride (DAB, Thermo Scientific). Finally, sections were counterstained with hematoxylin for 30 s. After staining, sections were dehydrated sequentially in 70%, 95%, and 100% ethanol then treated with xylene. All Ab16831 sections were coverslipped using Permount and dried in a chemical fume hood for three days. Quantitation of Ab16831-positive staining was performed using a StereoInvestigator system. Regions of interest were drawn around the individual cells. Cells containing SOD1 within the grey matter were normalized to the total area quantified. Each section was quantified twice and the average of the two counts were used. Other antibodies were visualized by fluorescence microscopy.

Fluorescence microscopy. Both primary antibodies C4F6 and 10C12 were visualized using an Alexa-Fluor-488-conjugated fluorescent anti-mouse secondary antibody. Anti-Iba1 was visualized using an Alexa-Fluor-594 anti-guinea pig secondary antibody. Nuclei were counterstained with 4',6-diamidino-2-phenylindole (DAPI). Images were acquired using a Keyence BZ9000 fluorescence microscope. The central aspect of the spinal cord was used to define the area analyzed and background fluorescence was eliminated using the background-reduction function in the software controlling the microscope. Quantification of integrated fluorescence per unit area (in μm^2) was done using ImageJ (53).

Statistical Analysis. All statistical analyses were performed using Prism 7.0d (GraphPad Software). To identify differences among groups, Student's t-test was used for female vs. male mouse group analysis and one-way analyses of variance (ANOVA) was used for comparison among treatment groups. $p < 0.05$ was considered statistically significant.

12

Associated content: Supporting information.

Conflict of interest: The authors declare no conflict of interest.

Author Contributions: RM, HM, and PW performed the experiments, CIC, NS, RSA, FGK, and TS provided critical reagents, GB and MW designed the study, MJS and JAL designed specific experiments, RM, HM, JAL, MW, and GB wrote the manuscript.

References

1. Chio, A., Logroscino, G., Traynor, B. J., Collins, J., Simeone, J. C., Goldstein, L. A., and White, L. A. (2013) Global epidemiology of amyotrophic lateral sclerosis: a systematic review of the published literature. *Neuroepidemiology* **41**, 118-130

2. Sreedharan, J., and Brown, R. H., Jr. (2013) Amyotrophic lateral sclerosis: Problems and prospects. *Ann Neurol* **74**, 309-316

3. Ratovitski, T., Corson, L. B., Strain, J., Wong, P., Cleveland, D. W., Culotta, V. C., and Borchelt, D. R. (1999) Variation in the biochemical/biophysical properties of mutant superoxide dismutase 1 enzymes and the rate of disease progression in familial amyotrophic lateral sclerosis kindreds. *Hum Mol Genet* **8**, 1451-1460

4. Reaume, A. G., Elliott, J. L., Hoffman, E. K., Kowall, N. W., Ferrante, R. J., Siwek, D. F., Wilcox, H. M., Flood, D. G., Beal, M. F., Brown, R. H., Jr., Scott, R. W., and Snider, W. D. (1996) Motor neurons in Cu/Zn superoxide dismutase-deficient mice develop normally but exhibit enhanced cell death after axonal injury. *Nat Genet* **13**, 43-47

5. Johnston, J. A., Dalton, M. J., Gurney, M. E., and Kopito, R. R. (2000) Formation of high molecular weight complexes of mutant Cu, Zn-superoxide dismutase in a mouse model for familial amyotrophic lateral sclerosis. *Proc. Natl. Acad. Sci. USA*. **97**, 12571-12576

6. Siddique, T., and Ajroud-Driss, S. (2011) Familial amyotrophic lateral sclerosis, a historical perspective. *Acta myologica : myopathies and cardiomyopathies : official journal of the Mediterranean Society of Myology / edited by the Gaetano Conte Academy for the study of striated muscle diseases* **30**, 117-120

7. Martin D, Thompson MA, and Nadler JV. (1993) The neuroprotective agent riluzole inhibits release of glutamate and aspartate from slices of hippocampal area CA1. *European Journal of Pharmacology* **250**, 473-476

8. Sawada, H. (2017) Clinical efficacy of edaravone for the treatment of amyotrophic lateral sclerosis. *Expert Opin Pharmacother* **18**, 735-738

9. Liu, T., and Bitan, G. (2012) Modulating self-assembly of amyloidogenic proteins as a therapeutic approach for neurodegenerative diseases: strategies and mechanisms. *ChemMedChem* **7**, 359-374

10. Xia, G., Benmohamed, R., Kim, J., Arvanites, A. C., Morimoto, R. I., Ferrante, R. J., Kirsch, D. R., and Silverman, R. B. (2011) Pyrimidine-2,4,6-trione derivatives and their inhibition of mutant SOD1-dependent protein aggregation. Toward a treatment for amyotrophic lateral sclerosis. *Journal of medicinal chemistry* **54**, 2409-2421

11. Trippier, P. C., Zhao, K. T., Fox, S. G., Schiefer, I. T., Benmohamed, R., Moran, J., Kirsch, D. R., Morimoto, R. I., and Silverman, R. B. (2014) Proteasome activation is a mechanism for pyrazolone small molecules displaying therapeutic potential in amyotrophic lateral sclerosis. *ACS Chem. Neurosci.* **5**, 823-829

12. Nowak, R. J., Cuny, G. D., Choi, S., Lansbury, P. T., and Ray, S. S. (2010) Improving binding specificity of pharmacological chaperones that target mutant superoxide dismutase-1 linked to familial amyotrophic lateral sclerosis using computational methods. *Journal of medicinal chemistry* **53**, 2709-2718

13. Rosen, D. R., Siddique, T., Patterson, D., Figlewicz, D. A., Sapp, P., Hentati, A., Donaldson, D., Goto, J., O'Regan, J. P., Deng, H. X., and et al. (1993) Mutations in Cu/Zn superoxide dismutase gene are associated with familial amyotrophic lateral sclerosis. *Nature* **362**, 59-62

14. Gurney, M. E., Pu, H., Chiu, A. Y., Dal Canto, M. C., Polchow, C. Y., Alexander, D. D., Caliendo, J., Hentati, A., Kwon, Y. W., Deng, H. X., and et al. (1994) Motor neuron degeneration in mice that express a human Cu,Zn superoxide dismutase mutation. *Science* **264**, 1772-1775

15. Kim, R. B., Irvin, C. W., Tilva, K. R., and Mitchell, C. S. (2015) State of the field: An informatics-based systematic review of the SOD1-G93A amyotrophic lateral sclerosis transgenic mouse model. *Amyotroph Lateral Scler Frontotemporal Degener*, 1-14

16. Attar, A., and Bitan, G. (2014) Disrupting self-assembly and toxicity of amyloidogenic protein oligomers by " molecular tweezers" – from the test tube to animal models. *Curr. Pharm. Des.* **20**, 2469-2483

17. Schrader, T., Bitan, G., and Klärner, F. G. (2016) Molecular tweezers for lysine and arginine - powerful inhibitors of pathologic protein aggregation. *Chem Commun (Camb)* **52**, 11318-11334

18. Malik, R., Di, J., Nair, G., Attar, A., Taylor, K., Teng, E., Klarner, F. G., Schrader, T., and Bitan, G. (2018) Using Molecular Tweezers to Remodel Abnormal Protein Self-Assembly and Inhibit the Toxicity of Amyloidogenic Proteins. *Methods Mol. Biol.* **1777**, 369-386

19. Sinha, S., Lopes, D. H., Du, Z., Pang, E. S., Shanmugam, A., Lomakin, A., Talbiersky, P., Tennstaedt, A., McDaniel, K., Bakshi, R., Kuo, P. Y., Ehrmann, M., Benedek, G. B., Loo, J. A., Klärner, F. G., Schrader, T., Wang, C., and Bitan, G. (2011) Lysine-specific molecular tweezers are broad-spectrum inhibitors of assembly and toxicity of amyloid proteins. *J. Am. Chem. Soc.* **133**, 16958-16969

20. Sinha, S., Du, Z., Maiti, P., Klärner, F. G., Schrader, T., Wang, C., and Bitan, G. (2012) Comparison of three amyloid assembly inhibitors: the sugar *scyllo*-inositol, the polyphenol epigallocatechin gallate, and the molecular tweezer CLR01. *ACS Chem. Neurosci.* **3**, 451-458

21. Zheng, X., Liu, D., Klärner, F. G., Schrader, T., Bitan, G., and Bowers, M. T. (2015) Amyloid β-protein assembly: The effect of Molecular Tweezers CLR01 and CLR03. *J Phys Chem B* **119**, 4831-4841

22. Prabhudesai, S., Sinha, S., Attar, A., Kotagiri, A., Fitzmaurice, A. G., Lakshmanan, R., Ivanova, M. I., Loo, J. A., Klärner, F. G., Schrader, T., Stahl, M., Bitan, G., and Bronstein, J. M. (2012) A novel "molecular tweezer" inhibitor of α-synuclein neurotoxicity in vitro and in vivo. *Neurotherapeutics* **9**, 464-476

23. Acharya, S., Safaie, B. M., Wongkongkathep, P., Ivanova, M. I., Attar, A., Klärner, F. G., Schrader, T., Loo, J. A., Bitan, G., and Lapidus, L. J. (2014) Molecular basis for preventing α-synuclein aggregation by a molecular tweezer. *J. Biol. Chem.* **289**, 10727-10737

24. Attar, A., Ripoli, C., Riccardi, E., Maiti, P., Li Puma, D. D., Liu, T., Hayes, J., Jones, M. R., Lichti-Kaiser, K., Yang, F., Gale, G. D., Tseng, C. H., Tan, M., Xie, C. W., Straudinger, J. L., Klärner, F. G., Schrader, T., Frautschy, S. A., Grassi, C., and Bitan, G. (2012) Protection of primary neurons and mouse brain from Alzheimer's pathology by molecular tweezers. *Brain* **135**, 3735-3748

25. Richter, F., Subramaniam, S. R., Magen, I., Lee, P., Hayes, J., Attar, A., Zhu, C., Franich, N. R., Bove, N., De La Rosa, K., Kwong, J., Klarner, F. G., Schrader, T., Chesselet, M. F., and Bitan, G. (2017) A Molecular Tweezer Ameliorates Motor Deficits in Mice Overexpressing α-Synuclein. *Neurotherapeutics* **14**, 1107-1119

26. Ferreira, N., Pereira-Henriques, A., Attar, A., Klärner, F. G., Schrader, T., Bitan, G., Gales, L., Saraiva, M. J., and Almeida, M. R. (2014) Molecular tweezers targeting transthyretin amyloidosis. *Neurotherapeutics* **11**, 450-461

27. Xu, N., Bitan, G., Schrader, T., Klarner, F. G., Osinska, H., and Robbins, J. (2017) Inhibition of Mutant alphaB Crystallin-Induced Protein Aggregation by a Molecular Tweezer. *J Am Heart Assoc* **6**, e006182

28. Chattopadhyay, M., Durazo, A., Sohn, S. H., Strong, C. D., Gralla, E. B., Whitelegge, J. P., and Valentine, J. S. (2008) Initiation and elongation in fibrillation of ALS-linked superoxide dismutase. *Proc. Natl. Acad. Sci. USA* **105**, 18663-18668

29. Hallewell, A. R., Mills, R., Tekamp-Olson, P., Blacher, R., Rosenberg, S., Ötting, F., Masiarz, F. R., and Scandella, C. J. (1987) Amino terminal acetylation of authentic human Cu,Zn superoxide dismutase produced in yeast. *Bio/Technology* **5**, 363–366

30. Giehm, L., and Otzen, D. E. (2010) Strategies to increase the reproducibility of protein fibrillization in plate reader assays. *Anal Biochem* **400**, 270-281

31. Vöpel, T., Bravo-Rodriguez, K., Mittal, S., Vachharajani, S., Gnutt, D., Sharma, A., Steinhof, A., Fatoba, O., Ellrichmann, G., Nshanian, M., Heid, C., Loo, J. A., Klärner, F. G., Schrader, T., Bitan, G., Wanker, E. E., Ebbinghaus, S., and Sanchez-Garcia, E. (2017) Inhibition of Huntingtin Exon-1 Aggregation by the Molecular Tweezer CLR01. *J. Am. Chem. Soc.* **139**, 5640-5643

32. Nshanian, M., Lantz, C., Wongkongkathep, P., Schrader, T., Klärner, F. G., Ehrmann, M., Smet-Nocca, C., Bitan, G., and Loo, J. A. (2018) Native Top-Down Mass Spectrometry and Ion Mobility Spectrometry of the Interaction of Tau Protein with a Molecular Tweezer Assembly Modulator. Submitted for publication

33. Nshanian, M., Lantz, C., Wongkongkathep, P., Schrader, T., Klarner, F. G., Blumke, A., Despres, C., Ehrmann, M., Smet-Nocca, C., Bitan, G., and Loo, J. A. (2018) Native Top-Down Mass Spectrometry and Ion Mobility Spectrometry of the Interaction of Tau Protein with a Molecular Tweezer Assembly Modulator. *J Am Soc Mass Spectrom*

34. Rakhit, R., and Chakrabartty, A. (2006) Structure, folding, and misfolding of Cu,Zn superoxide dismutase in amyotrophic lateral sclerosis. *Biochim. Biophys. Acta* **1762**, 1025-1037

35. Attar, A., Chan, W. T., Klärner, F. G., Schrader, T., and Bitan, G. (2014) Safety and pharmacological characterization of the molecular tweezer CLR01 – a broad-spectrum inhibitor of amyloid proteins' toxicity. *BMC Pharmacol. Toxicol.* **15**, 23

36. Capote, J., Kramerova, I., Martinez, L., Vetrone, S., Barton, E. R., Sweeney, H. L., Miceli, M. C., and Spencer, M. J. (2016) Osteopontin ablation ameliorates muscular dystrophy by shifting macrophages to a pro-regenerative phenotype. *J Cell Biol* **213**, 275-288

37. Brooks, S. P., and Dunnett, S. B. (2009) Tests to assess motor phenotype in mice: a user's guide. *Nat Rev Neurosci* **10**, 519-529

38. Heiman-Patterson, T. D., Deitch, J. S., Blankenhorn, E. P., Erwin, K. L., Perreault, M. J., Alexander, B. K., Byers, N., Toman, I., and Alexander, G. M. (2005) Background and gender effects on survival in the TgN(SOD1-G93A)1Gur mouse model of ALS. *J Neurol Sci* **236**, 1-7

39. Scott S, Kranz JE, Cole J, Lincecum JM, Thompson K, Kelly N, Bostrom A, Theodoss J, Al-Nakhala BM, Vieira FG, Ramasubbu J, and Heywood JA. (2008) Design, power, and interpretation of studies in the standard murine model of ALS. *Amyotrophic Lateral Sclerosis* **9**, 4-15

40. Nichols, N. L., Van Dyke, J., Nashold, L., Satriotomo, I., Suzuki, M., and Mitchell, G. S. (2013) Ventilatory control in ALS. *Respir Physiol Neurobiol* **189**, 429-437

41. Bosco, D. A., Morfini, G., Karabacak, N. M., Song, Y., Gros-Louis, F., Pasinelli, P., Goolsby, H., Fontaine, B. A., Lemay, N., McKenna-Yasek, D., Frosch, M. P., Agar, J. N., Julien, J. P., Brady, S. T., and Brown, R. H., Jr. (2010) Wild-type and mutant SOD1 share an aberrant conformation and a common pathogenic pathway in ALS. *Nat. Neurosci.* **13**, 1396-1403

42. Brotherton, T. E., Li, Y., Cooper, D., Gearing, M., Julien, J. P., Rothstein, J. D., Boylan, K., and Glass, J. D. (2012) Localization of a toxic form of superoxide dismutase 1 protein to pathologically affected tissues in familial ALS. *Proc. Natl. Acad. Sci. USA.* **109**, 5505-5510

43. Atlasi, R. S., Malik, R., Corrales, C. I., Tzeplaeff, L., Whitelegge, J. P., Cashman, N. R., and Bitan, G. (2018) Investigation of Anti-SOD1 Antibodies Yields New Structural Insight into SOD1 Misfolding and Surprising Behavior of the Antibodies Themselves. *ACS Chem. Biol.* **13**, 2794-2807

44. Ivanova, M. I., Sievers, S. A., Guenther, E. L., Johnson, L. M., Winkler, D. D., Galaleldeen, A., Sawaya, M. R., Hart, P. J., and Eisenberg, D. S. (2014) Aggregation-triggering segments of SOD1 fibril formation support a common pathway for familial and sporadic ALS. *Proc. Natl. Acad. Sci. USA.* **111**, 197-201

45. Ida, M., Ando, M., Adachi, M., Tanaka, A., Machida, K., Hongo, K., Mizobata, T., Yamakawa, M. Y., Watanabe, Y., Nakashima, K., and Kawata, Y. (2016) Structural basis of Cu, Zn-superoxide dismutase amyloid fibril formation involves interaction of multiple peptide core regions. *J Biochem* **159**, 247-260

46. van Es, M. A., Dahlberg, C., Birve, A., Veldink, J. H., van den Berg, L. H., and Andersen, P. M. (2010) Large-scale SOD1 mutation screening provides evidence for genetic heterogeneity in amyotrophic lateral sclerosis. *J Neurol Neurosurg Psychiatry* **81**, 562-566

47. Hilton, J. B., Mercer, S. W., Lim, N. K., Faux, N. G., Buncic, G., Beckman, J. S., Roberts, B. R., Donnelly, P. S., White, A. R., and Crouch, P. J. (2017) Cu(II)(atsm) improves the neurological phenotype and survival of SOD1(G93A) mice and selectively increases enzymatically active SOD1 in the spinal cord. *Sci. Rep.* **7**, 42292

48. Talbiersky, P., Bastkowski, F., Klärner, F. G., and Schrader, T. (2008) Molecular clip and tweezer introduce new mechanisms of enzyme inhibition. *J. Am. Chem. Soc.* **130**, 9824-9828

49. Gralla, E. B., and Valentine, J. S. (1991) Null mutants of Saccharomyces cerevisiae Cu,Zn superoxide dismutase: characterization and spontaneous mutation rates. *J Bacteriol* **173**, 5918-5920

50. Wei, J. P., Srinivasan, C., Han, H., Valentine, J. S., and Gralla, E. B. (2001) Evidence for a novel role of copper-zinc superoxide dismutase in zinc metabolism. *J. Biol. Chem.* **276**, 44798-44803

51. Hayward, L. J., Rodriguez, J. A., Kim, J. W., Tiwari, A., Goto, J. J., Cabelli, D. E., Valentine, J. S., and Brown, R. H., Jr. (2002) Decreased metallation and activity in subsets of mutant superoxide dismutases associated with familial amyotrophic lateral sclerosis. *J. Biol. Chem.* **277**, 15923-15931

52. Rogers, D. R. (1965) Screening for amyloid with the Thioflavin-T fluorescent method. *American Journal of Clinical Pathology* **44**, 59-61

53.   Abramoff, M. D., Magelhaes, P. J., and Ram, S. J. (2004) Image Processing with ImageJ. *Biophotonics Intl.* **11**, 36-42

FOOTNOTES

The abbreviations used are: ALS, amyotrophic lateral sclerosis; ANOVA, analysis of variance; DAB, 3,3'- diaminobenzidine tetrahydrochloride; DAPI, 4',6-diamidino-2-phenylindole; EM, electron microscopy; ESI, electrospray ionization; fALS, familial ALS; IHC, immunohistochemistry; i.p., intraperitoneal; MS, mass spectrometry; MS/MS, tandem mass spectrometry; NGS, normal goat serum; s.c., subcutaneous; SOD1, Cu-Zn superoxide dismutase; TCEP, tris(2-carboxyethyl)phosphine; ThT, thioflavin T; WT, wild-type
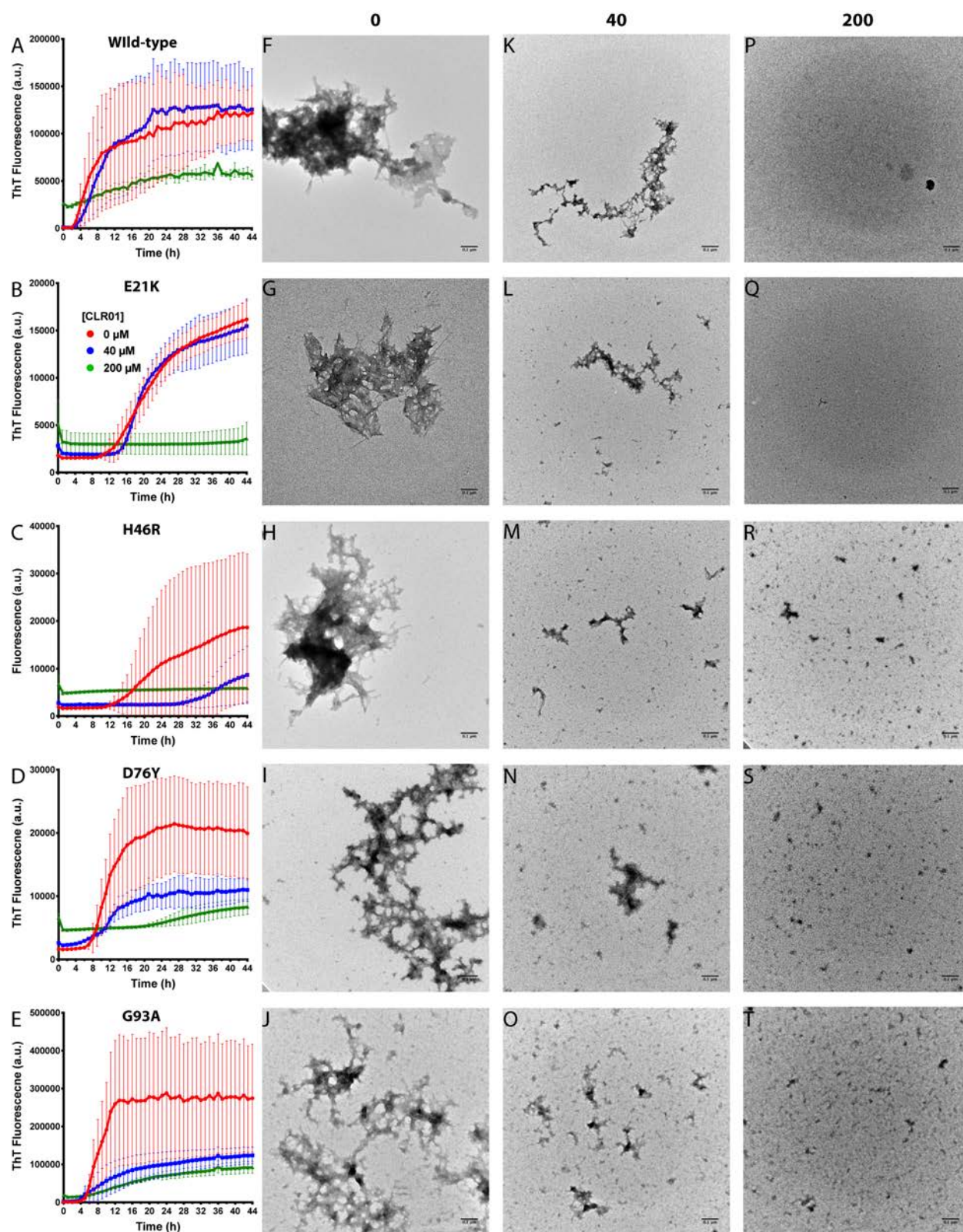
Figure 1. CLR01 inhibits SOD1 aggregation in vitro. A–E) Aggregation kinetics was measured using the ThT fluorescence assay. Wild-type SOD1 (A), or the variants E21K (B), H46R (C), D76Y (D), G93A (E) each were incubated at 40 μM in the absence or presence of 40 or 200 μM

19

CLR01. F–T) The morphology of the protein was examined at the end of each aggregation reaction by EM. Scale bars denote 0.1 μm.
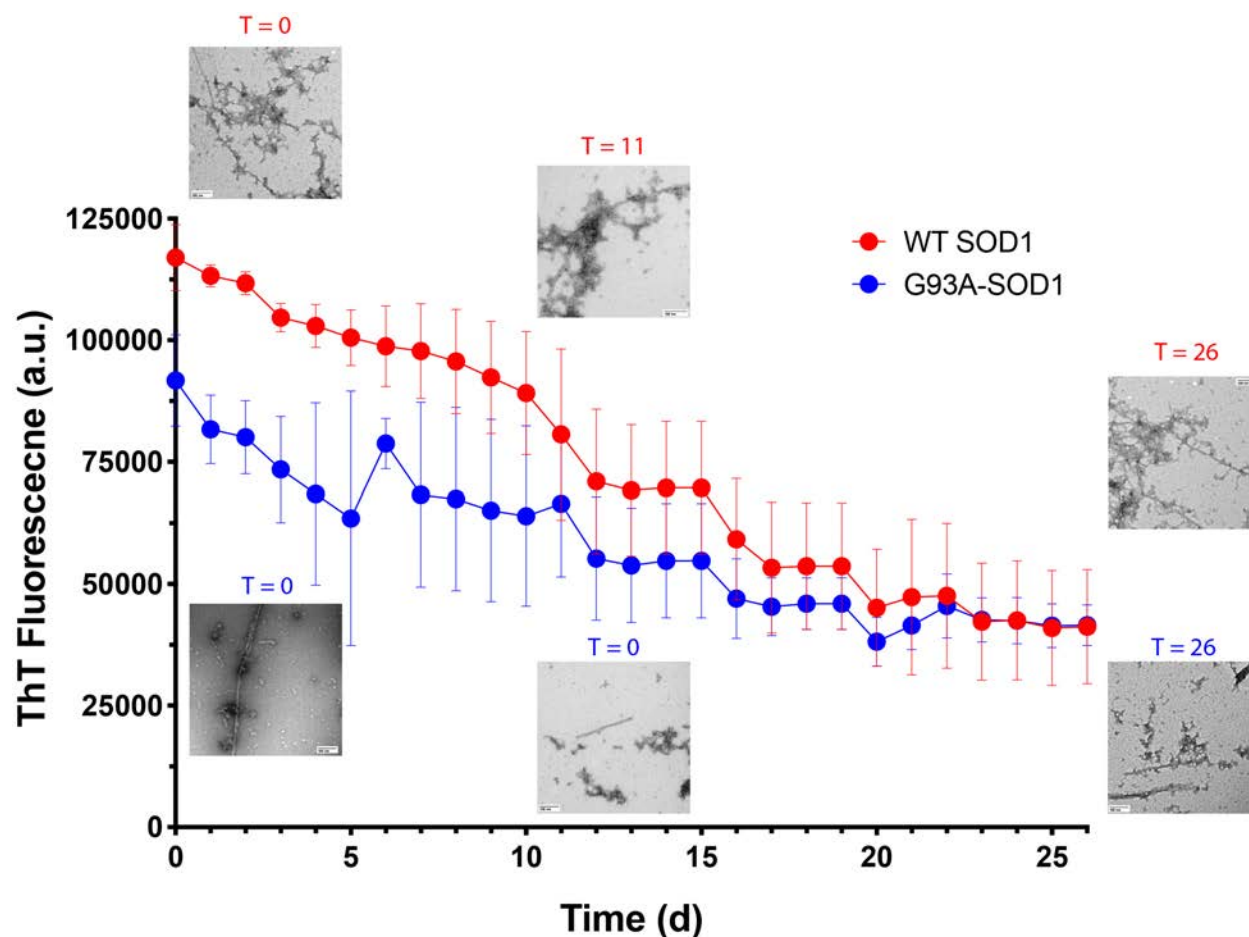

Figure 2. CLR01 partially disrupts the cross-β structure in pre-formed SOD1 aggregates. Forty-μM WT SOD1 or G93A-SOD1 were aged for 6 months and then incubated with 400 μM CLR01 in the presence of ThT and the fluorescence was monitored every day for 26 days. Aliquots were taken in the beginning of the reaction (day 0), after 10 days, and at the end of the reaction (day 26) and examined by EM.
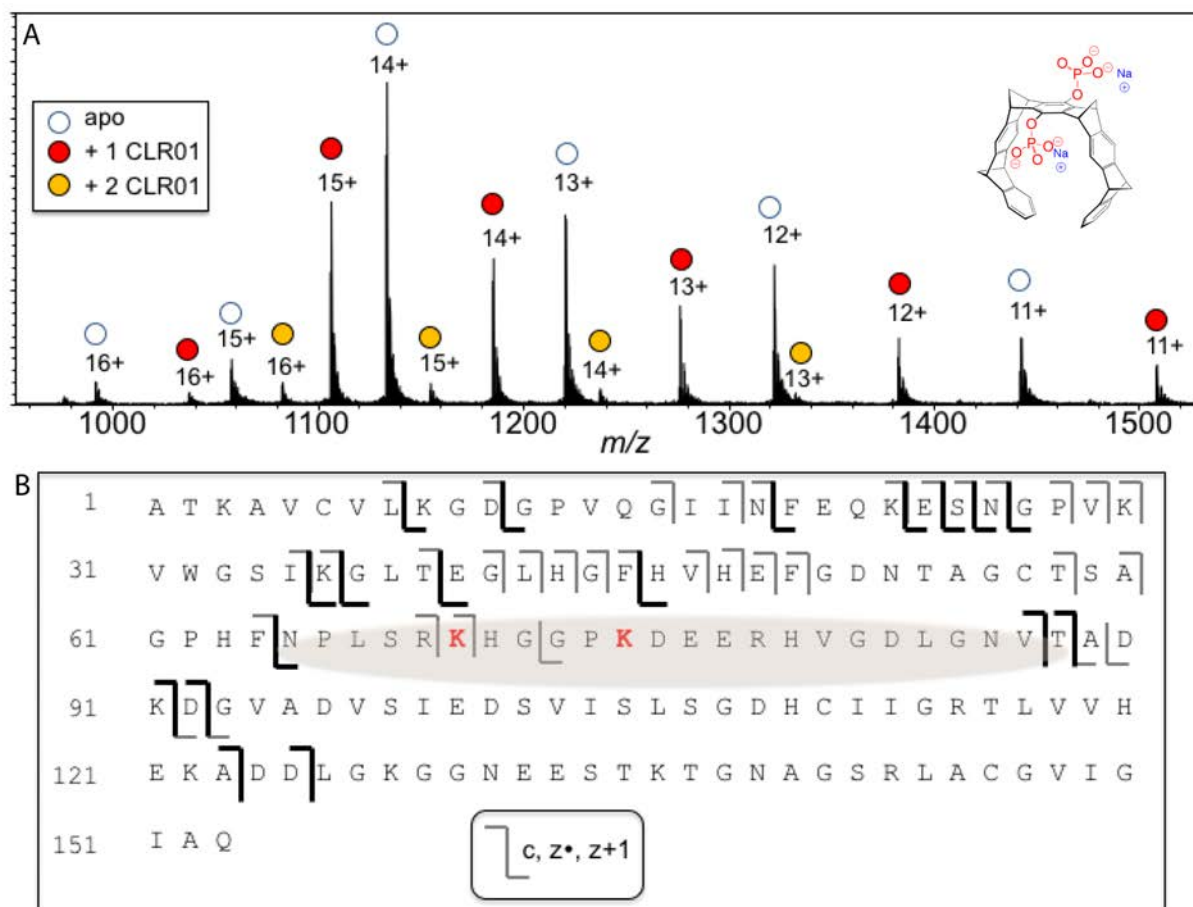
Figure 3. Binding of CLR01 on SOD1 investigated by ESI-MS. A) An ESI mass spectrum of a 10-μM SOD1 / 10-μM CLR01 mixture shows predominantly a 1:1 binding stoichiometry. The structure of CLR01 is shown at the top right corner. B) Schematic of the ECD-MS/MS fragmentation profile for the 12+-charged 1:1 SOD1:CLR01 complex. Product ions that retained binding to CLR01 are shown in dark colored lines. From the fragmentation profile, the shaded region is suggested to be the site(s) of CLR01 binding.
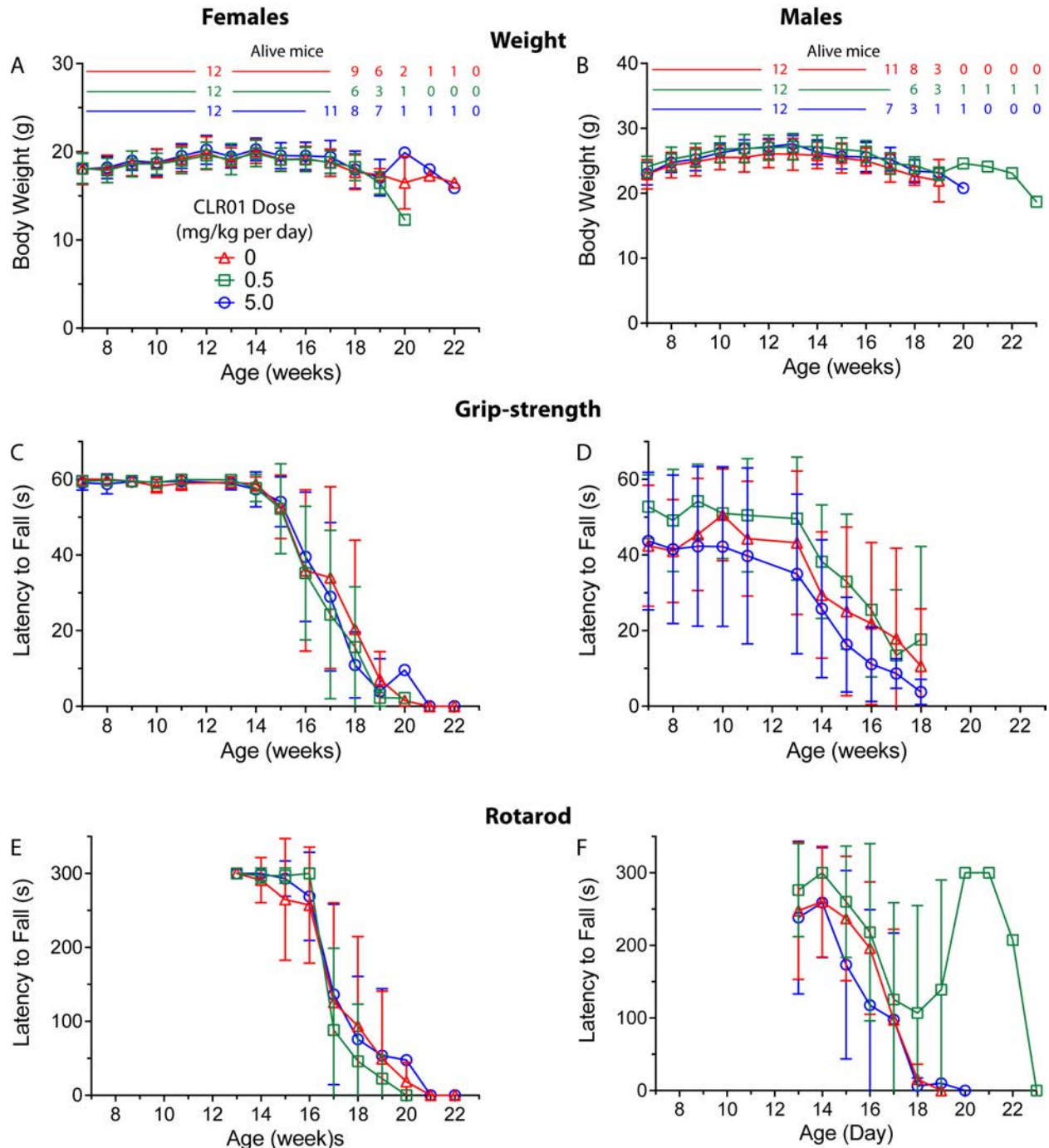
Figure 4. CLR01 treatment did not affect mouse weight or motor performance significantly. Male and female (n = 12 per group each) SOD1-G93A transgenic mice were administered a daily s.c. dose of saline vehicle or CLR01 (0.5 or 5 mg/kg) from 50 days of age until meeting criteria for euthanasia. Body weight (A, B) and grip-strength (C, D) were monitored weekly starting on week 7 and rotarod performance (E, F) was tested weekly starting on week 13 (E, F). The key in panel A is applicable to all the other panels. The number of animals used to calculate the average and SD at each time point is shown above panels A and B using the same color code and are applicable also to panels C–F. To facilitate comparison among the three measurements, all the graphs are shown with the same time scale. Missing data points in panel D were not recorded.
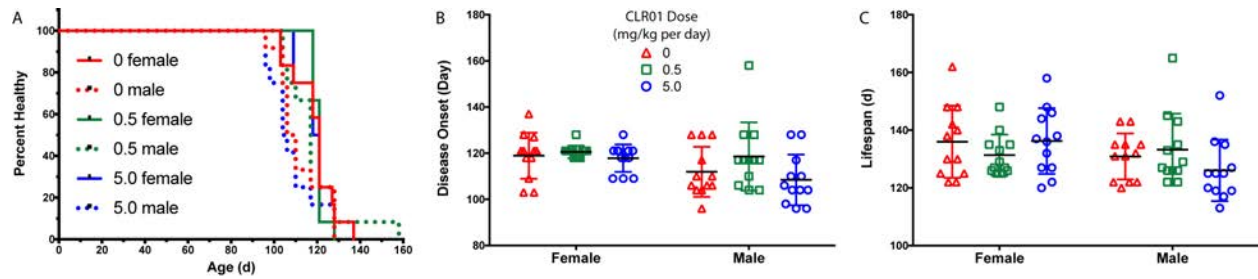
Figure 5. CLR01 did not increase G93A-SOD1 mouse survival. A) A Kaplan-Meier analysis of disease onset in male and female (n = 12 per group each) G93A-SOD1 mice. B) Disease onset was determined on the day of the first sign of weakness—crossing of hindlegs when mice were lifted by the tail. C) Lifespan represents the day the mouse either died or met criteria for euthanasia. The key in panel B is applicable also to panel C.
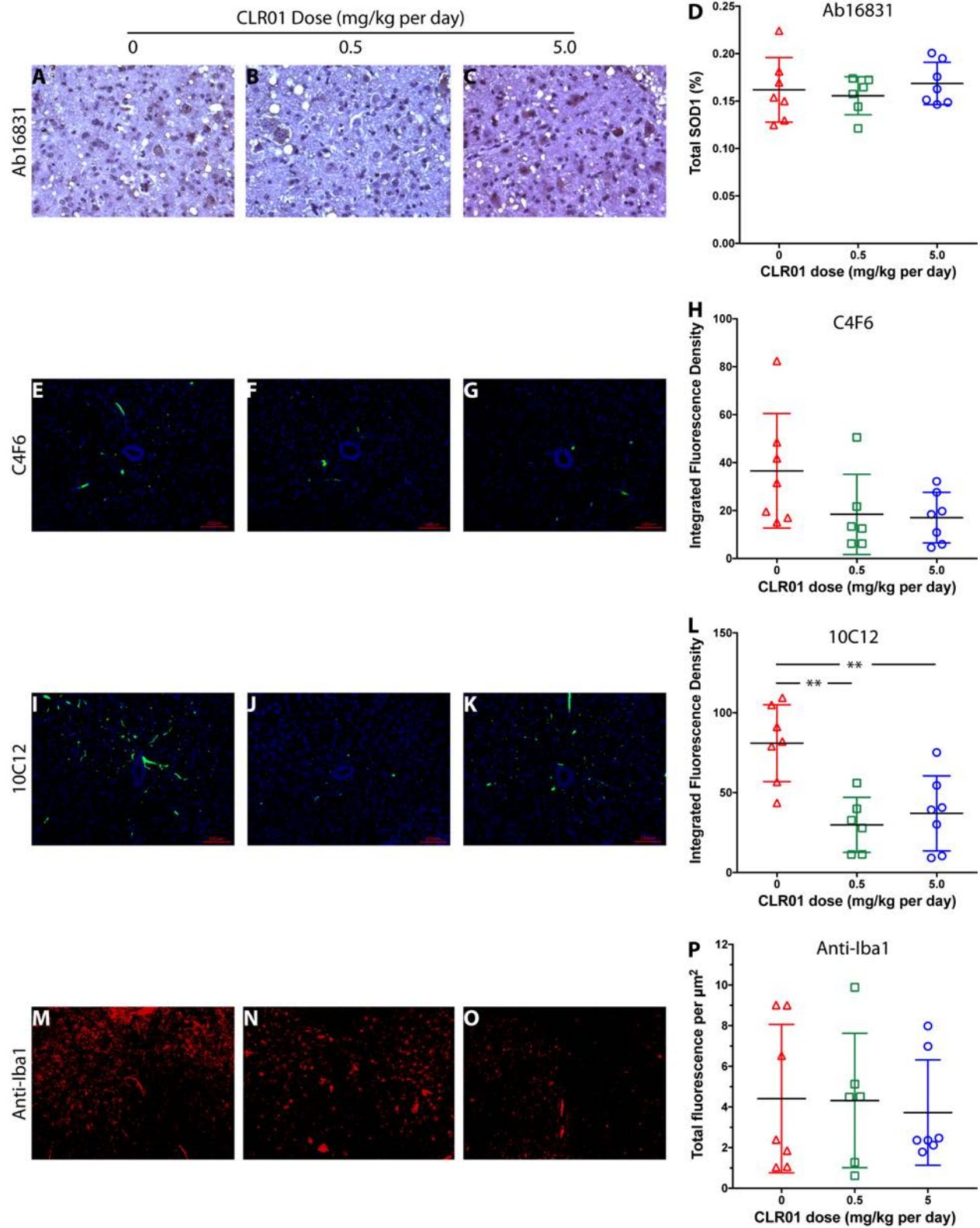
Figure 6. Analysis of SOD1 and microglia in mouse spinal cord. Lumbar spinal cord sections from euthanized mice were analyzed by IHC. A–C) Representative images of pAb 16831, a pan-SOD1 antibody, staining for total mouse and human SOD1 in A) vehicle-, B) 0.5-, and C) 5.0-

24

mg/kg CLR01-treated mice. D) Quantitative analysis of pAb 16831 staining. E-H) Representative images of mAb C4F6, which stains specifically apo G93A-SOD1 in E) vehicle-, F) 0.5-, and G) 5.0-mg/kg CLR01-treated mice. H) Quantitative analysis of mAb C4F6 staining. I–L) Representative images of mAb 10C12, which stains specifically early-forming species of misfolded SOD1 in I) vehicle-, J) 0.5-, and K) 5.0-mg/kg CLR01-treated mice. L) Quantitative analysis of mAb 10C12 staining. M–P) Representative images of anti-Iba1 pAb, which stains microglia in M) vehicle-, N) 0.5-, and O) 5.0-mg/kg CLR01-treated mice. P) Quantitative analysis of anti-Iba1 staining. The scale bars in panels E–G and I–K denote 100 µm and are applicable also to panels M–O. **$p < 0.01$, 1-way ANOVA with *post hoc* Tukey test.

The molecular tweezer CLR01 inhibits aberrant superoxide dismutase 1 (SOD1) self-assembly in vitro and in the G93A-SOD1 mouse model of ALS

Ravinder Malik, Helen Meng, Piriya Wongkongkathep, Christian I. Corrales, Niki Sepanj, Ryan S. Atlasi, Frank-Gerrit Klärner, Thomas Schrader, Melissa J Spencer, Joseph A. Loo, Martina Wiedau and Gal Bitan

Access the most updated version of this article at doi: 10.1074/jbc.RA118.005940

Alerts:
- When this article is cited
- When a correction for this article is posted

Click here to choose from all of JBC's e-mail alerts